Manuscript Details

Manuscript number	COMNET_2019_1305_R1
Title	Impulse Response Analysis of an Ultrasonic Human Body Channel
Article type	Research Paper

Abstract

Ultrasounds have been successfully and safely employed in underwater communications and for health diagnosis in the last 60 years because of their good performance in environments with high water concentration. Recently it has been proposed also to employ them for supporting intra-body communications; however exploitation of ultrasounds inside the body calls for a deep understanding of their features and a full characterization of the impulse response inside these challenging channels. In this paper we provide a complete experimental characterization of the impulse response inside a human body communication channel, composed for more than 65-70\% of water. To this purpose we developed a testbed which employs a human phantom of ballistic gel to emulate the human body propagation features and performed a set of measurements to fully discuss the channel behavior as a function of different parameters such as the employed frequency, the channel composition and the distance. Our results show that, it is possible to clearly identify the three main components generated by multipath propagation inside the human phantom, i.e. the direct, lateral and reflected waves. Also, it is possible to observe that the excess delay which measures the time elapsed between the first and the last arriving waves, increases approximately as 10 μs per cm. Our analysis provides interesting has strong implications on the design of communication protocols for intra-body scenarios.

Keywords	BAN, channel impulse response, ultrasonic networks
Taxonomy	Communication Network Architecture, Wireless Network
Corresponding Author	Laura Galluccio
Corresponding Author's Institution	University of Catania
Order of Authors	Laura Galluccio, Elisabetta Sciacca
Suggested reviewers	Falko Dressler, Zhangyu Guan

Submission Files Included in this PDF

File Name [File Type]

risposte_revisori.pdf [Response to Reviewers]

paperCOMNET.pdf [Manuscript File]

BIOS.pdf [Author Biography]

PHOTOS.pdf [Author Photo]

COI.pdf [Conflict of Interest]

declaration-of-competing-interests.pdf [Author Statement]

Submission Files Not Included in this PDF

File Name [File Type]

paperCOMNET.tex [LaTeX Source File]

To view all the submission files, including those not included in the PDF, click on the manuscript title on your EVISE Homepage, then click 'Download zip file'.

Research Data Related to this Submission

There are no linked research data sets for this submission. The following reason is given:
The authors do not have permission to share data

Impulse Response Analysis of an Ultrasonic Human Body Channel

Elisabetta Sciacca and Laura Galluccio
CNIT Research Unit, Dipartimento di Ingegneria Elettrica Elettronica e Informatica
University of Catania, Italy
Email: {name.surname}@unict.it

Abstract

Ultrasounds have been successfully and safely employed in underwater communications and for health diagnosis in the last 60 years because of their good performance in environments with high water concentration. Recently it has been proposed also to employ them for supporting intra-body communications; however exploitation of ultrasounds inside the body calls for a deep understanding of their features and a full characterization of the impulse response inside these challenging channels. In this paper we provide a complete experimental characterization of the impulse response inside a human body communication channel, composed for more than 65-70% of water. To this purpose we developed a testbed which employs a human phantom of ballistic gel to emulate the human body propagation features and performed a set of measurements to fully discuss the channel behavior as a function of different parameters such as the employed frequency, the channel composition and the distance. Our results show that, it is possible to clearly identify the three main components generated by multipath propagation inside the human phantom, i.e. the direct, lateral and reflected waves. Also, it is possible to observe that the excess delay which measures the time elapsed between the first and the last arriving waves, increases approximately as 10 μs per cm. Our analysis provides interesting has strong implications on the design of communication protocols for intra-body scenarios.

Keywords: BAN, ultrasonic networks, channel impulse response.

1. Introduction

Ultrasounds have been used in several applications over time. In the last century, as an example, ultrasounds have raised interest for communication purposes. During the World War I, Allies developed the first SONAR (SOund Navigation And Ranging) [1] and developed an underwater communication system for military applications to counteract German submarines.

In 1942 ultrasounds were used for the first time on human tissues for diagnostic and therapeutic purposes localizing brain tumors [2]. After that, ultrasounds have been exploited in many other medical fields. Their main well-known application is represented by imaging techniques; since the 1930s they have been also used for therapeutic purposes. Ultrasounds have been employed, for example, in the treatment of Meniere disease for the destruction of the vestibular nerve, or also in Parkinson disease therapy where are employed for localized brain tissue destruction.

Nowadays, it is widely recognized that therapies exploiting ultrasounds are safe and do not exhibit dangerous counter-effects or cause damage to body tissues. In [3] a rich overview of therapeutic applications of ultrasounds is presented.

Only recently, the idea of employing ultrasonic communications inside the body which, similarly to underwater channels, is composed for more than 65-70% of water, has been proposed with a focus on e-health applications.
This idea is reinforced by the inadequate performance of traditional RF communication and its potential healthy risks. In fact, studies in [4] and [5] revealed that ultrasonic communications require much lower transmission power with respect to the low-power RF-based technology as water aids the propagation of ultrasonic waves and hinders the RF transmission. This leads to lower energy per bit cost and longer links supported.
However in order to perform efficient ultrasonic communications inside the body, a deep understanding of the peculiar features of this channel is needed. To our knowledge this detailed characterization of the impulse response inside the human body channel has not been derived so far. Accordingly, in this paper, we present an experimental characterization of the impulse response inside a human body channel. In order to perform such characterization we develop a testbed which employs a human phantom of ballistic gel to mimic the human body propagation features and perform a set of measurements to fully describe the channel behavior as a function of the employed frequency, the composition of the medium and the distance. Our investigation shows that, it is possible to clearly identify the 3 main components generated by multipath propagation inside the human phantom which are associated to the direct, lateral and reflected waves. Also, it is possible to observe that the excess delay, which measures the time elapsed between the first and the last arriving waves, increases approximately as 10 μs per cm. Moreover we study the behavior of the attenuation (i.e. the modulus channel gain) depending on the frequency and show that an appropriate choice of the transmission frequency allows to minimize the channel attenuation. Impact of channel heterogeneity due to tissues and bones is also investigated showing that it only increases the standard deviation of the gain modulus due to multipath, but does not increase in general the average values. Our analysis provides, thus, interesting implications on the design of communication protocols for intra-body scenarios by considering jointly the path loss and the delay spread.

The rest of this paper is organized as follows. In Section 2 relevant literature in the field is discussed. In Section 3 some basics of ultrasounds physics are introduced and in Section 4 the main features of a ultrasonic transducer are recalled. In Section 5 the impulse response model for the channel under consideration is derived and the measurement procedure carried out is described in Section 6. In Section 7 numerical results are illustrated and, finally, in Section 9, concluding remarks are drawn.

2. Related Work

The use of ultrasonic communications for health monitoring and diagnosis has been proposed in the last years by different research groups. Indeed, together with the use of ultrasounds in early diagnosis of fetus during pregnancy, it was also proposed to employ them for communications inside the human body.
In 2008 for the first time Infantis and Kalis proposed a simple propagation model exploring the theoretical feasibility of using ultrasounds inside the body [6]. In the same line of reasoning, in 2012 Santagati et al. published two papers ([7] and [8]) presenting a detailed discussion on important tradeoffs regarding the frequency range, the transmission power, the bandwidth and

the transducers' features.
Two years later the same authors developed the first simple prototype of a software-defined testbed architecture providing an experimental demonstration of the feasibility of employing ultrasonic communications into human body [9]. In the same year, also an hybrid opto-acoustic communication among nanorobots was proved [10].
These feasibility studies were independently confirmed by Dressler, Charthad and Singer in 2015 and 2016, respectively. In particular, the first paper addressed the control and communication problem between intrabody nanosensors and an external unit [11]. Charthad, instead, showed the implementation of a mm-sized implantable device using ultrasonic power transfer and a hybrid bi-directional data communication link [12]. Similarly other studies assessing the possibility to use ultrasonic waves inside the human body appeared [13]. Finally Singer [14] showed an experimental acoustic transmission through real pork tissues and beef liver achieving data rates up to 20-30 Mbps with QAM modulation. On the same line of reasoning, in [15] the use of different modulation schemes was considered in order to identify which mechanism performs better in a variable frequency range, up to approximately 400 kHz. In 2017, in [16], [17] it was demonstrated for the first time also the possibility of using multihop communications with four ultrasonic nodes communicating through a human body phantom containing organic tissues (chicken bone, muscles and skin). In the same year, in [16], the tissue overheating problem is faced for the first time and a thermal aware routing protocol is proposed.

Different research groups have also focused their efforts on identification of communication schemes for this peculiar environment. In 2015, for the first time, Guan et al. considered the problem of designing optimal network control algorithms for distributed networks like BANs. They proposed lightweight, asynchronous, and distributed algorithms for either rate control or stochastic channel access designed to maximize the throughput under energy constraints ([18, 19]). On the other hand, in [20] the authors proposed an Ultrasonic WideBand (UsWB) transmission scheme combined with a multiple access technique, based on the idea of transmitting information bits spread over very short pulses in a time-hopping pattern.
In [21] and [22] also other communication schemes and error control strategies are discussed.
In [23] it was also proposed to employ ultrasounds at the nanoscale to design a hierarchical Body Area Nano-Network (BANN) architecture consisting of two types of devices, nanonodes and nanorouter which operate in the THz band. In particular a human hand scenario is considered by taking also into account the impact of path loss and molecular absorption noise.

However, in order to proceed with the implementation and development of real acoustic body area networks, a proper channel impulse response analysis is still needed. In [24] for the first time a simple channel model based on simulation and in-vivo experimental measurements is discussed.
Later, in 2016, Rivet et al. developed a near and far field model based on a simulated body channel [4]. More recent works such as [25] and [26], instead presented a more detailed characterization of channels for frequencies up to 2 MHz.
Based on the above considerations it is evident that a deep understanding of the acoustic channel response at frequencies higher than 2 MHz and for distances longer than few centimeters is still missing and will be the focus of this work.

3. Ultrasounds Physics

Similar to light, acoustic vibrations which are mechanical perturbations, travel in the form of a wave. However, although other waves, like light waves, can travel in vacuum, acoustic waves

require an elastic medium such as a liquid or a solid to propagate.
With respect to the entire acoustic spectrum, ultrasounds are mechanical vibrations covering frequencies greater than 20 kHz, thus far beyond the range of human hearing.
In our previous work [20] we have investigated on the suitable range of frequencies to support transmission in tissues. In particular we have identified that, given that attenuation and frequency are inversely proportional, depending on tissues features, there is a maximum allowed carrier frequency for a given maximum tolerable attenuation. In particular, in order to guarantee a suitable communication distance, at least in the order of tens of centimeters, we observed that the transmission frequency should not exceed 10 MHz. Similar results were also derived independently in [27]. Accordingly, in this paper we will consider the 1-5 MHz spectrum range because it represents a good trade-off between the need for having a reasonable attenuation, as discussed above, and the need for not increasing excessively the transducer size as discussed in the following.

Propagation of acoustic and, specifically, ultrasonic waves, is impacted by numerous features. At a high level, the main problems exhibited during pressure wave propagation can be classified in:

- *attenuation* of the transmitted signals which is related to the absorption of sound waves in media and, specifically, in environments with high water concentration;
- *perturbation and deformation* of the signal which propagates due to variations in the sound speed related to the heterogeneous medium and reflections on the material surfaces which also cause strong multi-path, thus generating parasite echoes and interference;
- *environmental noise inside the body* due to biological mechanisms ongoing inside the body.

The above features result in absorption, reflection, scattering, refraction, diffraction and interference which require appropriate design and consideration.

- *Absorption* is the process by which a material takes part of the sound wave energy and transforms it into heat. This obviously introduces a loss into the wave propagation process;
- *Reflection* is the process by which a sound wave is back-propagated because there is a change in the direction of the wavefront at an interface between two different media. Reflection can be specular or diffuse depending on if the reflected wave is characterized by a single direction or not. Acoustic impedance impacts on this process;
- *Scattering* causes a redistribution of the acoustic energy among different wave numbers and frequencies resulting in spectral and directional broadening of the waves at sufficiently high frequencies;
- *Refraction* corresponds to a change of directivity of a sound beam induced by the mean velocity gradient of the flow;
- *Diffraction* occurs when the sound wave meets a large obstacle so that there is a shadow behind where the incident wave cannot penetrate deeply;
- *Interference* occurs when acoustic sources emit waves of the same frequency and their distance is a multiple of the wavelength, so interference appears where the waves are superimposed.

In the following wave propagation and particle motion will be described.

3.1. Wave Propagation and Particle Motion

Acoustic wave propagation consists of a sequence of compressions and dilatations in an elastic medium. The propagation rate of the consequent medium perturbation is denoted as *acoustic wave velocity*. The propagation velocity of an acoustic wave depends on the propagation medium as

$$c = \sqrt{\frac{E}{\rho}} \tag{1}$$

where E is the elastic modulus, and quantifies the relative variation of volume or density as a function of pressure variations, and ρ is the medium density.

At a given temperature and pressure, for a certain point in space, the velocity c in a perfectly elastic material is independent of temperature and pressure , i.e. $c(T, p) = c$, and the relationship between the velocity, the frequency f and wavelength of a wave λ is:

$$\lambda = \frac{c}{f} \tag{2}$$

However, an ultrasonic source generates more than one mechanical wave. In particular, one can distinguish four different types of waves (Figure 1):

- The *Longitudinal wave* that is a compression wave in which the particle motion and the propagation of the wave do have the same direction;
- The *Shear wave* where the particle motion and the direction of the propagation are perpendicular;
- The *Surface (Rayleigh) wave* that travels across the surface of a material and has an elliptical particle motion. Its depth of penetration is approximately equal to one wavelength and the velocity is approximately 90% of the shear wave velocity of the material;
- The *Love wave* that has a complex vibration and is parallel to the plane layer, perpendicular to the wave direction.

All these waves induce pressure variations over the three dimensions and can be fully described by the Helmholtz equation:

$$\nabla^2 P - \frac{1}{c^2}\frac{\partial^2 P}{\partial t^2} = 0 \tag{3}$$

where $P(x, y, z, t)$ is the pressure field of a wave propagating in space as a function of time and $c(x, y, z)$ is the local material propagation velocity which, in general, can be dependent on the position.

If the ultrasonic wave encounters an absorbing medium, the initial pressure P_0 decays by following the relationship:

$$P(d) = P_0 e^{-\beta d} \tag{4}$$

where d is the distance and β is the amplitude attenuation coefficient.

Clearly, in case of non-isotropic environments, multiple set of waves appear due to multipath fading. Their number and entities are related to the particular scattering phenomenon generated in the material.

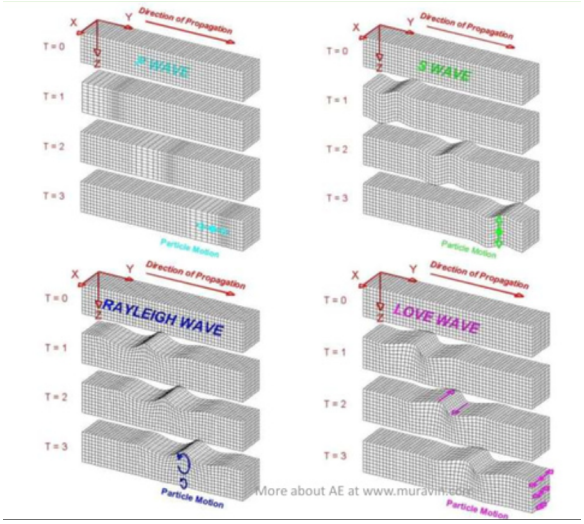

Figure 1: a) Longitudinal (particle motion and wave propagation in the same direction), b) Shear (orthogonal particle motion and wave propagation) , c) Rayleigh (elliptical particle motion and wave propagation across the surface) and d) Love (particle motion parallel to the plane layer and orthogonal to wave propagation) waves ([28]).

4. The Ultrasonic Transducer

An ultrasonic transducer is a device used to generate and detect ultrasonic waves. Different types of ultrasonic transducers are available in the market, depending on the specific application they are designed for. Contact, immersion, and air-coupled transducers are some of the most common types of ultrasonic devices employed for the majority of applications and differ mainly for the coupling media employed between the transducer and the sample. Contact transducers employ a highly viscous fluid for coupling so that a reduced mismatch between the impedance of the tested material and the transducer is achieved; immersion transducers use instead water for coupling. Air-coupled transducers instead use air as the medium for the waves to propagate.

The use of a transducer implies a good knowledge of its physics. Each of its parameters influences the propagation of acoustic waves inside the material.

In Figure 2, the main components of a generic ultrasonic transducer are shown. In particular an active element, a backing and a wear plate are needed while the core of the device consists of the active element where a piezo or ferroelectric material trasduces the electrical energy into a mechanical wave.

Once the ultrasonic wave leaves the wear plate, two regions of propagation can be distinguished: the near field (or Fresnel zone) and the far field (or Fraunhofer zone).

In the near field a series of maxima and minima of the echo amplitude occur until the last maximum is reached, at distance N (see Figure 3).

Then, in the far field, the beam profile spreads and the sound field pressure gradually decreases.

The near field distance from the transducer N depends on the transducer diameter D, the propagation velocity of the acoustic wave c and f as follows:

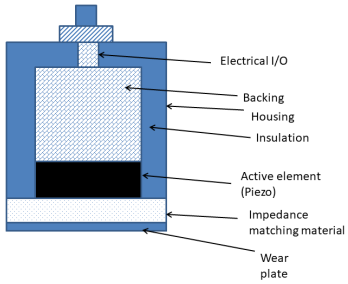

Figure 2: Main components of an acoustic transducer.

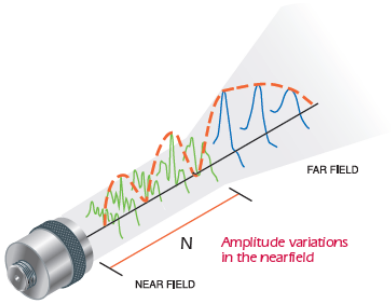

Figure 3: Near and Far Field [29].

$$N = \frac{D^2 f}{4c} \tag{5}$$

According to eq. (5) note that the higher the frequency or the transducer diameter are, the larger the near field region size will be.

The beam spread in the far field can be also characterized using its angle of divergence for non focused transducer; the latter can be calculated from the following equation:

$$\sin \frac{\gamma}{2} = \frac{0.514v}{fD} \tag{6}$$

where $\frac{\gamma}{2}$ is the half -6dB angle spread.
This angle measures the divergence of the beam from the central axis to the point where the sound pressure has decreased by one half (-6 dB). The shape of the beam and, in particular, the near and far field regions for a particular material, can thus be tuned appropriately as a function of the size of the transducer and the frequency being used.

5. Channel Characterization

In order to completely characterize the wireless ultrasonic channel in this section we derive the impulse response. As in other wireless channels, this can be mathematically modeled as a linear filter with a complex low pass equivalent impulse response in the form of [30, 20]:

$$h(t) = \sum_{l}^{L} \alpha_l \delta(t - \tau_l) \tag{7}$$

where α and τ are the complex gain and delay for each of the l replicas and L is the overall number of replicas due to the presence of multipath, i.e. $l \in \{1 \dots L\}$. Indeed, during propagation of waves inside the medium, at least 3 components can be identified:

- *Direct wave*, which travels through the medium in Line-of-Sight (LoS) from the transmitter to the receiver;
- *Lateral wave*, which propagates out of the medium, along the external surface and, then, enters the medium to reach the receiver;
- *Reflected wave*, which travels through the medium and is reflected at the interface between the medium and other tissues such as bones, muscles or the external air.

Accordingly, in eq. (7), among the L components we will denote L_D the number of direct wave components, L_R the number of reflected components and L_L the number of lateral components, each characterized by its own gain and delay.

Another important parameter used to characterize a channel is the *path loss*, defined (in logarithmic form) as the difference between the transmitted power at the output of the transmission system and the received power at the output of the receiver antenna, before entering into the receiver circuit (in logarithmic form), i.e.

$$PL = P_t - P_r \tag{8}$$

In the above eq. (8), the received power[1] is given (in logarithmic form) as the sum of the received power due to the 3 types of waves (i.e. direct, reflected and lateral waves) and thus

$$P_r = \sum_{l_D}^{L_D} |\alpha_{l_D}|^2 + \sum_{l_R}^{L_R} |\alpha_{l_R}|^2 + \sum_{l_L}^{L_L} |\alpha_{l_L}|^2 \tag{9}$$

In order to derive the channel impulse response, the *excess delay* and the *mean excess delay* are useful metrics which can be derived. The former quantifies the time elapsed between the first and the last arriving components, while the latter is the first moment of the power delay profile and can be derived as:

$$\tau = \frac{\sum_k P_k \tau_k}{\sum_k P_k} \tag{10}$$

[1] We are assuming that $P_t = 1$ W.

where τ_k is the delay of the k-th replica and P_k is the associated instantaneous power.
Finally, also the *root mean square (RMS) delay spread* is calculated to give a complete description of the channel. This parameter is considered as a good indicator of multipath spread, because it gives hints on the occurrence of a possible inter-symbol interference (ISI).
The RMS delay spread is defined as:

$$\tau_{RMS} = \sqrt{(\tau^2) - (\tau)^2} \tag{11}$$

where (τ^2) is

$$(\tau^2) = \frac{\sum_k P_k \tau_k^2}{\sum_k P_k} \tag{12}$$

and τ_k is the associated delay for the k-th replica. Once we have defined the above metrics, in the following sections we will detail the experimental procedure carried out to derive in a real setting the channel impulse response.

6. Measurement Procedure

The measurement procedure required use of a set of laboratory instruments. The signal input is provided by an Agilent 33220A waveform generator [31] that produces a 10 V peak-to-peak Voltage pulse with 9% duty cycle and null offset. Via BNC connections, this pulse is delivered to a V326-SU Olympus transducer [29] that emits the resulting ultrasonic wave through an artifical human body mimicking phantom. The latter consists of 10% ballistic gelatin, used to mimic human muscle tissues [32]; we also considered a set of experiments where an animal bone is encapsulated in the gel in order to test also a more realistic scenario for BANs [2]. Many studies has been conducted about ultrasounds propagation speed in phantom tissues. Based on experiments described in [33], [34] and [35] it has been observed that the ballistic gel sound velocity is slightly lower than in water, exhibiting values around $1450\,\mathrm{m\,s^{-1}}$.
The ultrasonic pulse propagates inside the gel block in such a way to generate multiple copies as foreseen and discussed above. Then, a receiving transducer located at the opposite side of the ballistic gel block, sends the received signal to a Mini-Circuits ZFL-1000LN+ Low Power Amplifier (LNA) [36] connected to a Keysight Infiniium oscilloscope 900A series oscilloscope [37].
It estimates the amplitude and the delay of the received pulse. An illustrative example of the laboratory setup is shown in Figure 4.
In order to control the overall system we used the National Instrument LabVIEW software [38] to develop a customized Virtual Instrument (VI) to control either the waveform generator and the oscilloscope. In Figure 5 the front panel of our VI is shown.

In particular, the VI sets the generation of a pulse train with a particular frequency and queries the oscilloscope about the received amplitude. The frequency varies from 1 MHz to 5 MHz with a 1 kHz step. The choice of this set of frequencies is motivated by our preliminary work in [20, 8] where we showed that this range guarantees an appropriate tradeoff between a controllable size of the transducer (which could be in the long term also implanted), low tissue attenuation and a

[2] This work has respected the European Commission Guidelines on scientific activity involving animals. In particular, organic tissues (e.g. bones) have been obtained from those commercially available.

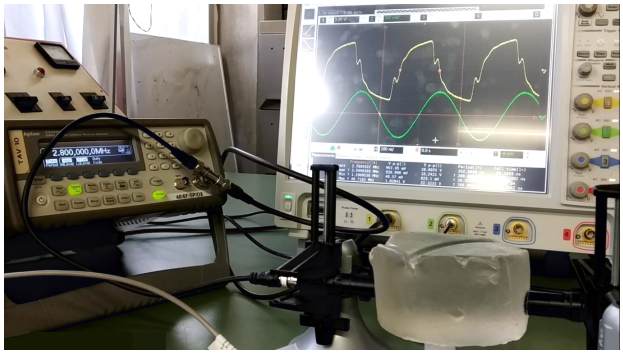

Figure 4: Experimental setting: Waveform generator, transmitter and receiver transducers, body phantom made of ballistic gel and oscilloscope.

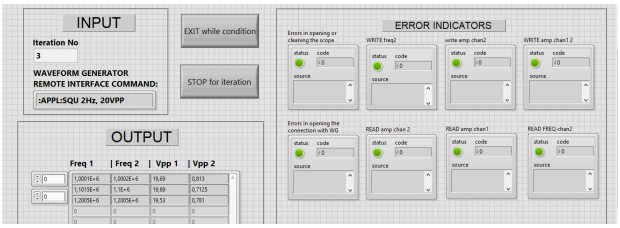

Figure 5: Customized Virtual Instrument developed in LabVIEW.

high directivity.
After repeating each set of measurements one hundred times, a table reporting the transmitted signal amplitude, the received signal amplitude and the frequency used for each iteration has been obtained.

We performed the measurement campaign in different settings. In particular, we varied the size and the composition of the medium considering a ballistic gel block with three possible diameters namely 5.5 cm, 10 cm and 12 cm; then, for each size, we considered not only the pure ballistic gel case, but also the condition where an animal bone 2 cm × 5 cm × 0.5 cm in size is encapsulated in the gel; our results provide an accuracy of 97.5%. Figure 6 illustrates the case with a ballistic gel block and a bone embedded.

The size of the block was chosen taking into account the transducer properties. Indeed, by remembering eq. (5) and given a transducer diameter of 952 mm [29], we calculated the N value for 3.7 MHz which is perfectly compatible with the central frequency declared in the transducer datasheet, by also taking into account that the presence of the LNA partially distorts the signal, thus reducing the central frequency with respect to the declared value. Accordingly, the desired near field distance is approximately 5.7 cm. The other block sizes (10 cm and 12 cm) were considered in order to test the possibility of communicating over longer distances.

Figure 6: Ballistic gel with bone embedded.

7. Numerical Analysis

In the following we will discuss the impact of channel composition and distance on different performance metrics such as delay and frequency response. Tables 1 and 2 summarize all the experimental parameters for each configuration. We will refer to them in the considerations below[3].

7.1. Impulse Response

In order to derive the impulse response we recall eq. (7), which can be characterized upon specifying the gain (α) and the delay (τ) associated to each replica.
In general, we send a pulse with 9% duty cycle and null offset; accordingly, the received signal consists of three multipath replicas, i.e. the direct, surface and reflected waves. When the last component exhibits a power level which is comparable with noise, the weak replica cannot be detected by the receiving transducer. This occurs when distances are large (e.g. 12 cm) or a heterogeneous channel (ballistic gel with bone) attenuates significantly the power of each component.
Figure 7 shows the modulus of the gain in case of homogeneous channel (i.e. pure ballistic gel) and a 10 cm gel block size. Note that the direct component reaches the transducer after 70.5 µs with a peak amplitude of −16.98 dB; the second component has a delay equal to 192 µs and its peak amplitude is −50.4 dB. Finally the last component arrives after 315.8 µs with a −53.36 dB peak amplitude.
Table 1 summarizes all α and τ values for the considered configurations.

7.2. Path Loss

In this section we investigate on the path loss. In particular, by calculating the path loss for each considered scenario, both Homogeneous and Heterogeneous channel, and with three different gel block sizes, we observed that, as expected, the path loss increases with distance and with

[3] In doing our experiments we assumed that a perfect matching of impedance happens and disregarded mismatch or microscopic phenomena that could arise in the derivation of the impulse response and all parameters discussed in the rest of this section.

Table 1: Gain module and delay of each component in all configurations

	5.5 cm				10 cm				12 cm			
	Homo		Hetero		Homo		Hetero		Homo		Hetero	
	α(dB)	Av τ(µs)	α(dB)	Av τ(µs)	α(dB)	Av τ(µs)	α(dB)	Av τ(µs)	α(dB)	Av τ(µs)	α(dB)	Av τ(µs)
1st component	-9.51	37.47	-14.90	29.46	-16.98	70.05	-17.21	68.82	-17.55	80	-25.43	84.36
2nd component	-52.39	112.8	-40.93	89.51	-50.4	192	-47.27	967.92	-41.98	240.76	N.A.	250
3rd component	N.A.	187	N.A.	N.A.	-53.36	315.8	N.A.	N.A.	N.A.	N.A.	N.A.	N.A.

Table 2: Main impulse response parameters for all configurations

	5.5 cm		10 cm		12 cm	
	Homogeneous	Heterogeneous	Homogeneous	Heterogeneous	Homogeneous	Heterogeneous
Path Loss (dB)	9.51	14.90	16.98	17.21	17.55	25.43
Excess Delay (µs)	75.33	60.05	121.95	899.1	160.76	165
# of replicas	3	2	3	2	2	2
τ (µs)	37.195 ± 0.27	29.595 ± 0.02	70.269 ± 0.005	69.624 ± 0.031	80.293 ± 0.03	83.545 ± 0.05
τ_{RMS} (µs)	6.4015 ± 0.0005	30.20 ± 0.04	6.512 ± 0.768	26.79 ± 0.02	6.922 ± 0.289	N.A.

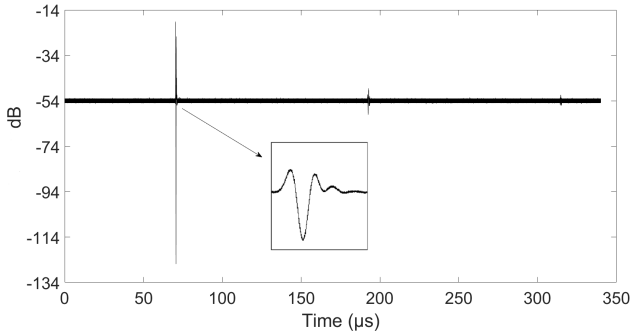

Figure 7: Modulus of the gain in case of homogeneous channel and 10 cm gel block size.

the addition of discontinuities in the medium.
As indicated in Table 2, in case of Homogeneous channel, the path loss seems to increase approximately at an average rate of 0.972 dB/cm.

The addition of a discontinuity element (i.e. heterogeneous case) makes the path loss decrease in a non-linear manner, reaching high values at larger distances. Note that in particular, at 12 cm, the gain modulus is −25.43 dBm while at 10 cm it was −17.21 dBm.

7.3. Excess Delay

In this paragraph we investigate on the excess delay which is defined as the time interval between the arrival of the first and the last signal components. Based on this definition, it is clear that the estimation of this parameter is affected by the number of copies obtained at the receiver. Accordingly, in order to take into account the lack of received components in case of larger distances, we considered only the time interval between the reception of the first and the second components. In case of Homogeneous channel, at 5.5 cm gel block size the excess delay is 75.33 μs, at 10 cm it is almost doubled, i.e. 121.95 μs, while for 12 cm the value of the excess delay is 160.7 μs. These values suggest that the excess delay increases approximately at a rate of 10.26 μs/cm.
Observe also that, as expected, the larger is the block size, and thus the distance between the transmitter and the receiver, the higher is the difference between the time employed by the direct wave to reach the destination and the time needed by the reflected components.

In case of Heterogeneous channel, the presence of scattering effects seems to make this parameter unpredictable with respect to distance. Indeed, the measured values of the excess delay are: 60.0 μs for 5.5 cm gel block size, 899.1 μs for 10 cm and 165 μs for 12 cm. Note that, in case of 10 cm, due to the unpredictable effects of a not perfectly identical positioning of the animal bone with respect to the other two cases, the scattered components are reflected multiple times, thus causing an excessive and unpredictable increase in the delay.

7.4. Mean Excess Delay

We have observed so far how the delay spread metrics are influenced by the number of copies received. Similar considerations can be done for the mean excess delay and for the RMS delay spread reported in Table 2.
Table 1 shows how τ depends on the number of replicas and the gel block size. Note that, the presence of discontinuity elements in the communication channel (i.e. heterogeneous case) does not necessarily correspond to an increased value of the mean excess delay. In fact, multipath copies could sum to superficial waves in a positive or destructive manner.
In Figure 8 we show the Cumulative Distribution Function of τ in case of 10 cm gel block size both for Homogeneous and for Heterogeneous channel. Note that the positive summing effect due to the presence of the discontinuity element at 10 cm is evident by observing the set of values of the mean excess delay. However note that the delay associated to the direct wave (i.e. the first component) is approximately unchanged.

7.5. RMS Delay Spread

In this paragraph experimental measurements on RMS delay spread are provided. From Table 2 observe that τ_{RMS} seems to slightly depend on the distance between transmitter and receiver, while it is mainly impacted by the channel composition.
Both for 5.5 cm and 10 cm block sizes, observe that the RMS delay in the homogeneous case is

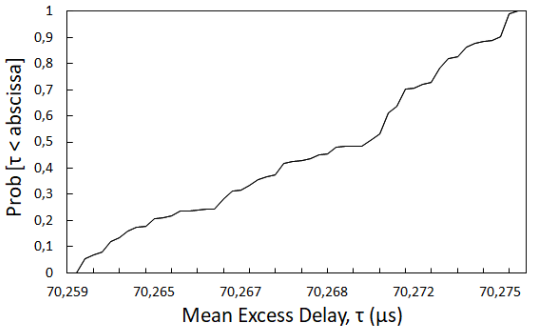

(a)

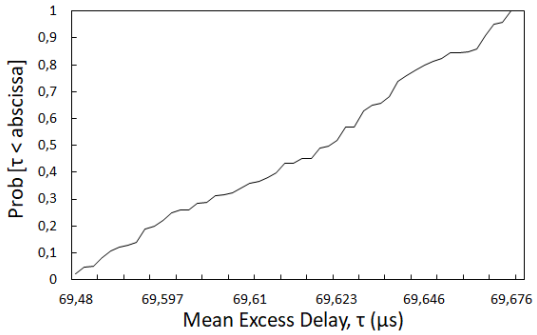

(b)

Figure 8: Distribution of Mean Excess Delay τ at 10 cm gel block size in both homogeneous (a) and heterogeneous (b) channels.

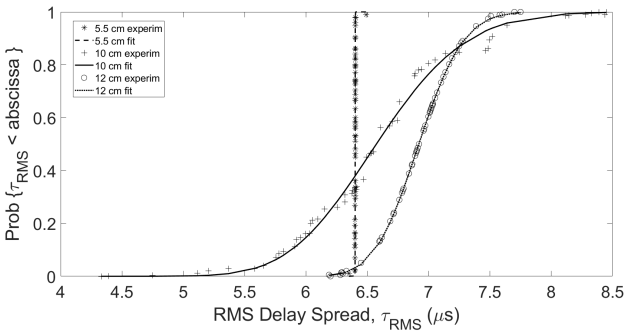

Figure 9: CDF of the RMS delay spread in case of homogeneous channel for 5.5 cm, 10 cm and 12 cm gel blocks.

about one fifth as compared to the heterogeneous case.
This means that the effect of having a homogeneous channel is to reduce the variability in the delay.

Unfortunately in case of 12 cm gel block size, the RMS for the heterogeneous case cannot be recorded because in this case only one component arrives at the receiver. As previously stated, in case of higher distances and heterogeneous channel, each component is heavily attenuated; so in this particular case, even the second component has a low amplitude, comparable with noise and, thus, cannot be recorded.

In Figure 9 we report the Cumulative Distribution Function of τ_{RMS} in case of homogeneous channel for 3 different gel block sizes. It is clear that at lowest distance this parameter is more stable showing a standard deviation σ equal to 0.0005 µs. This is because when the transmitter-receiver distance is low, in spite of the different path traveled by the three components, the delay remains limited. In the other cases instead, upon increasing the distance between the transmitter and the receiver, the difference in the traveled path becomes relevant and the RMS delay spread increases. In the extreme case when only 2 components are received (i.e. gel block size 12 cm), the RMS delay spread evaluation is imprecise and suffers for the lack of part of the delay contribution.

Note that in the same figure we also illustrate the comparison between the experimental data and the lognormal distribution. As evident, the RMS Delay Spread can be described quite well by the lognormal fit.

For the homogeneous channel described above, it is possible to calculate the coherence bandwidth of the channel which is proportional to the inverse of the RMS delay spread τ_{RMS}. Accordingly we could consider this channel as frequency- selective for signals of bandwidth above approximately 30 kHz [39].

7.6. Effect of Frequency

In this paragraph we perform an analysis of the gain modulus (i.e. $|\alpha|$) as a function of the frequency used.
In particular, we plot the transfer function modulus (i.e. the attenuation) depending on the frequency being selected in the experiments which has been chosen in the range 1.6-5MHz based on the considerations done in previous sections.

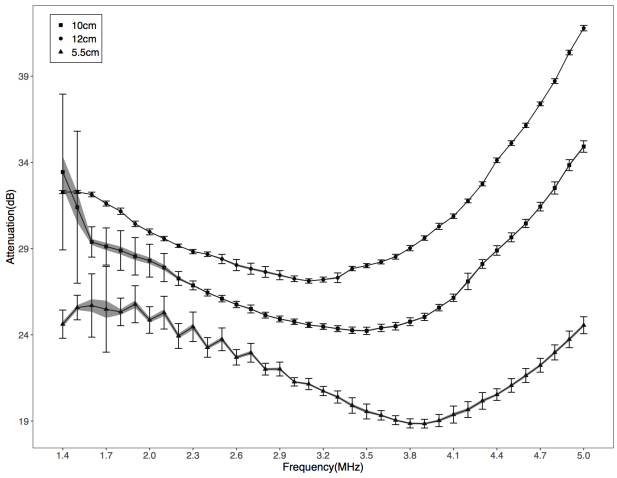

Figure 10: $|\alpha|$ Vs. Frequency in homogeneous channel when issuing a square pulse.

In Figures 10 and 12 we show $|\alpha|$ for each of the three gel block sizes considered, upon issuing either a square wave or a pulse. The square wave has 10 peak-to-peak Volt amplitude, 50% duty cycle and null offset. The pulse has 10 peak-to-peak Volt amplitude, 9% duty cycle, null offset. In the same plot we report also the standard deviation and the confidence interval (in grey color) set to 97.5%. In Figures 11 and 13 the same analysis is performed in case of heterogeneous channel.

By comparing Figures 10 and 11, as expected, we observe that the use of heterogeneous channels with a higher density causes an increase in $|\alpha|$. This is also evident by considering Figures 12 and 13. Note that, in case of a heterogeneous channel, also the standard deviation increases significantly, especially in case of 10 cm which has shown to be the most critical size for the gel block size. Also note that, due to the features of the ultrasonic transducer being employed, i.e. the V326-SU Olympus transducer, which has a maximum sensitivity at 3.4-3.5 MHz, $|\alpha|$ is minimal at these frequencies. We also observe that, due to the small coherence bandwidth, in case of pulse wave, the high signal frequency leads to larger variations in the attenuation.

8. Effect of propagation inside tissues

In this section we investigate on the dynamics of ultrasonic signal propagation inside tissues. Specifically we developed k-Wave simulations [40] of our testbed system consisting of a cylinder of ballistic gel with a bone embedded in it. In Figure 14 we show the considered topology, the signal received at different positions inside the bone, namely at the ingress of the bone, in the intermediate positions at 5 mm of distance each, till the egress of the bone. In Figures 15 (a) and (b) we observe the intensity of the received signal at the different positions inside the bone and at different time instants. Note that the maximum received signal intensity decreases upon moving rightmost inside the bone. This is because, as expected, the bone tissues add an attenuation to

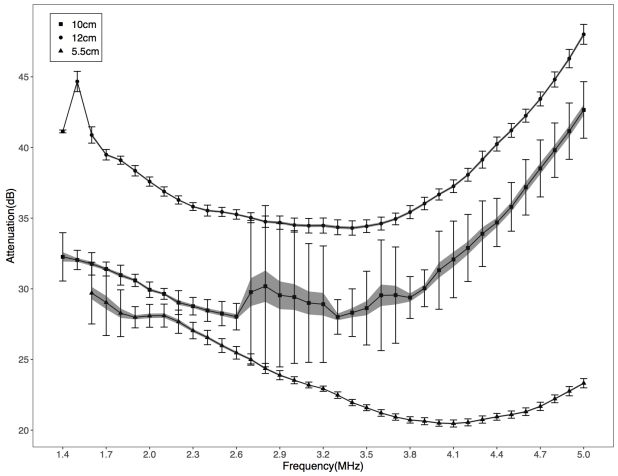

Figure 11: $|\alpha|$ Vs. Frequency in heterogeneous channel when issuing a square pulse.

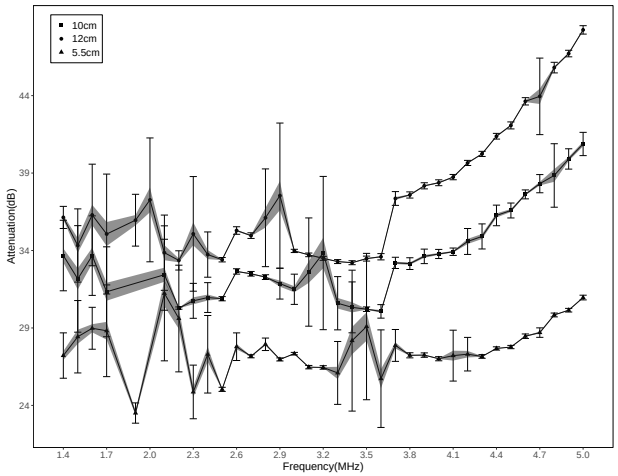

Figure 12: $|\alpha|$ Vs. Frequency in homogeneous channel when issuing a pulse.

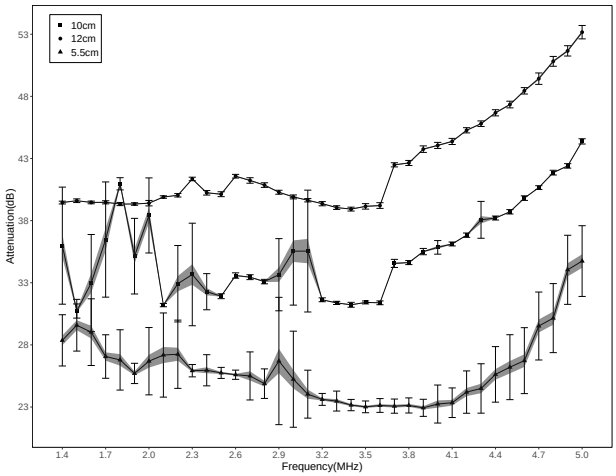

Figure 13: $|\alpha|$ Vs. Frequency in heterogeneous channel when issuing a pulse.

the signal. In Figure 15b a graphical representation of the intensity is shown with colors ranging from red to grey. Note the drastic decrease in the received signal at the different interfaces, in particular at the egress point of the bone.

In Figures 16 three snapshots report the ultrasonic acoustic field at different time instants and a different positions, inside the phantom and in proximity of the bone. Note that the effect of the presence of the bone is to cause numerous reflected waves and, thus, the presence of bone and similar heterogeneous tissues as compared to homogeneous ballistic gel, can turn into an advantage because it allows, through the existence of reflections, to propagate the signal also to far-away destinations.

9. Conclusions

In this paper, an analysis of the impulse response of a human body communication channel has been presented and assessed using experimental data. Distribution of mean excess delay and RMS delay spread has been investigated showing that they can be fitted by a lognormal distribution. We have discussed the effect of considering an homogeneous channel or a heterogeneous one where components with different densities have been added. Also the effect of transmitter-receiver distance has been investigated. The coherence bandwidth of the channel has been estimated in relationship with the RMS delay spread. The behavior of the channel at different frequency ranges has been studied as well as the propagation of the ultrasonic wave across heterogeneous tissues. Results provided in this work can be considered as a preliminary useful tool for the design and fully understanding of communication systems characterized by high water concentration. Our analysis can provide useful insights for the design of communication protocols for intra-body scenarios.

ACKNOWLEDGMENTS

Authors would like to thank our colleagues at the Measurement Systems Group at Dipartimento di Ingegneria Elettrica Elettronica e Informatica for the precious help in measurements

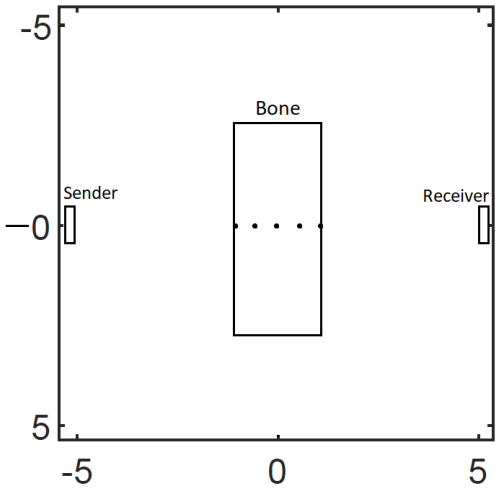

Figure 14: 2D topology considered for k-Wave simulations.

campaigns.

References

[1] X. Lurton. An introduction to underwater acoustics: Principles and Applications, 2002. Springer and Praxis Publishing.

[2] J. G. Lynn and R. L. Zwemer and A. J. Chick and A. E. Miller. A new method for the generation and use of focused ultrasound in experimental biology. *The Journal of General Physiology*, Vol. 26, pp. 179,193,1942.

[3] D. L. Miller et al. Overview of therapeutic ultrasound applications and safety considerations. *Journal of Ultrasound in Medicine* 31.4 (2012): 623-634.

[4] F. Rivet, S. Redois, and Y. Deval. Characterization of ultrasonic wave propagation for intra-body communication. 2016.

[5] G. E. Santagati and T. Melodia. An implantable low-power ultrasonic platform for the Internet of Medical Things. *IEEE INFOCOM 2017*.

[6] A. Ifantis and A. Kalis. On the use of ultrasonic communications in biosensor networks. *8th IEEE International Conference on BioInformatics and BioEngineering*. 2008.

[7] L. Galluccio, et al. Challenges and implications of using ultrasonic communications in intra-body area networks. *9th IEEE Annual Conference on Wireless On-Demand Network Systems and Services (WONS)*. 2012.

[8] G. E. Santagati, T. Melodia, L. Galluccio, S. Palazzo: Ultrasonic Networking for e-Health Applications, *IEEE Wireless Communications Magazine*, Special Issue on Wireless Networking for e-Health Applications, Vol. 20, n. 4, August 2013.

[9] G. E. Santagati, and T. Melodia. Sonar inside your body: Prototyping ultrasonic intra-body sensor networks. *IEEE INFOCOM 2014*.

[10] G. E. Santagati, and T. Melodia. Opto-ultrasonic communications for wireless intra-body nanonetworks. *Nano Communication Networks* 5.1-2 (2014), 3-14.

[11] F. Dressler, and S. Fischer. Connecting in-body nano communication with body area networks: Challenges and opportunities of the Internet of Nano Things. *Nano Communication Networks* 6.2 (2015): 29-38.

[12] J. Charthad, et al. A mm-sized implantable medical device (IMD) with ultrasonic power transfer and a hybrid bi-directional data link. . *IEEE Journal of solid-state circuits* 50.8 (2015): 1741-1753.

[13] D. Laqua and T. Shn and K. Kring and K. Albrecht and P.Husar. Ultrasound communication for intelligent implants. *Biomedical Engineering* Vol. 59, No. 1. 2014.

[14] A. Singer, M. Oelze, A. Podkowa. Mbps Experimental Acoustic Through-Tissue Communications: MEATCOMMS. *Proc. of SPAWC 2016.*

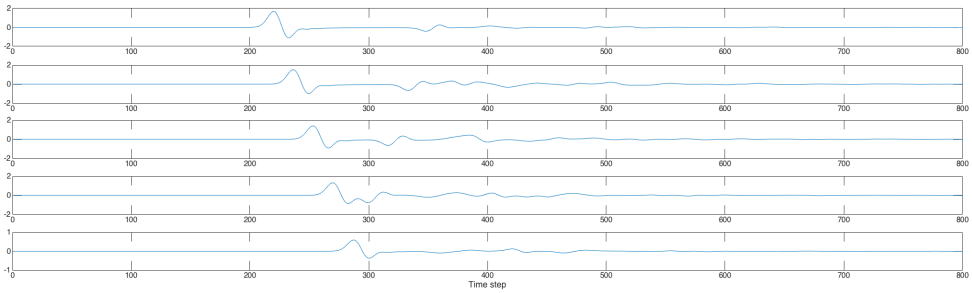

(a)

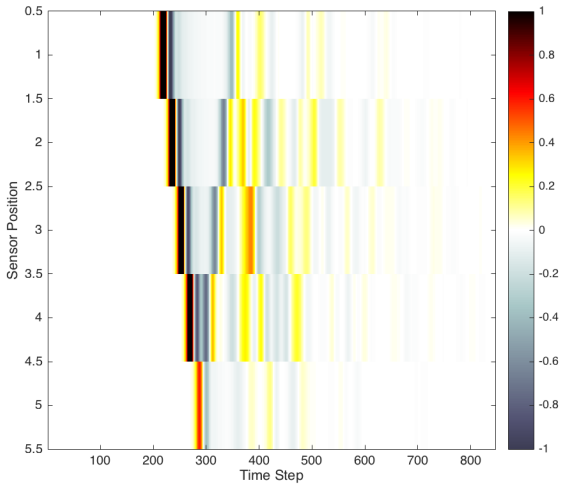

(b)

Figure 15: Received Ultrasonic Signal Intensity at different positions across the bone tissue as a function of time (a) and as a function of position and time (b).

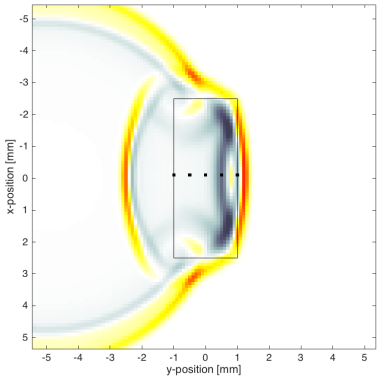

(a)

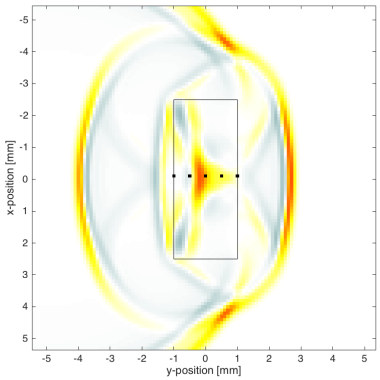

(b)

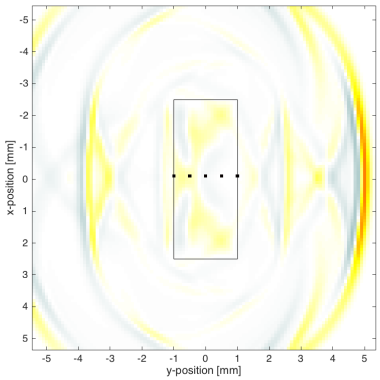

(c)

Figure 16: Ultrasonic field as a function of the distance traveled at three different time instants.

[15] M. Li, and Y. Kim. Feasibility Analysis on the Use of Ultrasonic Communications for Body Sensor Networks. *Sensors* 18.12 (2018): 4496.

[16] L. Galluccio, S. Milardo, and E. Sciacca. A feasibility analysis on the use of ultrasonic multihop communications for e-health applications. *IEEE ICC 2017*.

[17] L. Galluccio, S. Milardo, and E. Sciacca. Demo abstract an ultrasonic intra body area network for ehealth applications. *IEEE INFOCOM* 2017.

[18] G. Zhangyu, G. E. Santagati, and T. Melodia. Ultrasonic intra-body networking: Interference modeling, stochastic channel access and rate control. *IEEE INFOCOM* 2015.

[19] G. Zhangyu, G. E. Santagati, and T. Melodia. Distributed Algorithms for Joint Channel Access and Rate Control in Ultrasonic Intra-Body Networks. *IEEE/ACM Transactions on Networking* 24.5 (2016): 3109-3122.

[20] G. E. Santagati, T. Melodia, L. Galluccio, S. Palazzo. Medium access control and rate adaptation for ultrasonic intrabody sensor networks *IEEE Transactions on Networking* Vol. 23, No. 4. August 2015.

[21] E. Demirors, et al. High data rate ultrasonic communications for wireless intra-body networks. *IEEE LANMAN* 2016.

[22] M. Pratama, H. Bintang, et al. Implementation of ultrasonic communication for wireless body area network using amplitude shift keying modulation. *IEEE Region 10 Conference (TENCON)*, 2016.

[23] S. Canovas-Carrasco, A.-J. Garcia-Sanchez, and J. Garcia-Haro. A nanoscale communication network scheme and energy model for a human hand scenario *Elsevier nano communication networks* Vol. 15, March 2018.

[24] G. Wild, and S. Hinckley. Wireless acoustic communications for in-vivo biomedical device monitoring. *Biomedical Applications of Micro-and Nanoengineering IV and Complex Systems*. Vol. 7270. International Society for Optics and Photonics, 2008.

[25] W. Jiang, et al. Modelling of Channels for Intra-Corporal Ultrasound Communication. *IEEE International Ultrasonics Symposium (IUS)*, 2018.

[26] T. Bos, et al. Enabling Ultrasound In-Body Communication: FIR Channel Models and QAM Experiments. *IEEE Transactions on Biomedical circuits and systems*, 13.1 (2018): 135-144.

[27] T. Hogg and R. A. Freitas. Acoustic communication for medical nanorobots. *Nano Commun. Networks*. Vol. 3, No. 2, pp. 83-102. Jun. 2012.

[28] [Online]. Available: *https://www.slideshare.net/mboria/muravin-acoustic-emission-wave-propagation-and-source-location*

[29] Ultrasonic Tranducers Olympus V326-SU. [Online]. Available: *https://www.olympus-ims.com/it/ultrasonic-transducers/immersion/#!cms[focus]=descU8423054*

[30] A. Salam, M. C. Vuran, S. Irmak. Pulses in the Sand: Impulse Response Analysis of Wireless Underground Channel. *IEEE INFOCOM*, 2016.

[31] Agilent 33220A 20 MHz Waveform Generator. [Online]. Available: *https://web.sonoma.edu/esee/manuals/33220-90002.pdf*

[32] Ballistic Gelatin - Clear Ballistic. [Online]. Available: *https://www.clearballistics.com/shop/10-ballistic-gelatin-fbi-block/*

[33] Othman, Nur Shakila, et al. Ultrasound propagation speed of polymer gel mimicked human soft tissue in 23 days. *International Conference on Biomedical Engineering and Technology*. 2011.

[34] C. J. Shepherd, et al. The dynamic behaviour of ballistic gelatin. *AIP Conference Proceedings*. Vol. 1195. No. 1. AIP, 2009.

[35] J. Winter, and D. Shifler. The material properties of gelatin gels. MARVALAUD INC WESTMINSTER MD, 1975.

[36] Mini-Circuits Low Noise Amplifiers ZFL-1000LN+. [Online]. Available: *https://ww2.minicircuits.com/pdfs/ZFL-1000LN+.pdf*

[37] Keysight Infiniium Oscilloscopes - 900A series. [Online]. Available: *https://www.keysight.com/en/pcx-x205195/infiniium-90000a-series-oscilloscopes?cc=IT&lc=ita*

[38] NI LabVIEW Software. [Online]. Available: *http://www.ni.com/en-us/shop/labview.html*

[39] T. Rappaport. Wireless Communications: Principles and Practice. Upper Saddle River, NJ, USA: Prentice-Hall, 1999.

[40] k-Wave Matlab toolbox. *http://www.k-wave.org*

Laura Galluccio received her laurea degree in Electrical Engineering from University of Catania, Catania, Italy, in 2001. In March 2005 she got her Ph.D. in Electrical, Computer and Telecommunications Engineering at the same university under the guidance of Prof. Sergio Palazzo. Since 2002 she is also at the Italian National Consortium of Telecommunications (CNIT), where she worked as a Research Fellow within the VICOM (Virtual Immersive Communications) and the SATNEX Projects. Since November 2010 to October 2019 she has been Assistant Professor at University of Catania. From November 2019 she is Associate Professor at the same university. Her research interests include ad hoc and sensor networks, protocols and algorithms for wireless networks, and network performance analysis. From May to July 2005 she has been a Visiting Scholar at the COMET Group, Columbia University, NY under the guidance of Prof. Andrew T. Campbell. In September 2015 she has been Visiting Professor at Central Supelec, Gif-sur-Yvette, Paris. She is senior member of the IEEE.

Elisabetta Sciacca received her laurea degree in Telecommunications Engineering from University of Catania, in 2016. She is PhD Student in Complex systems for Physical, Socio-Economic and Life Science at University of Catania and currently Visiting PhD Student at the Centre for Translational Bioinformatics, Queen Mary University of London.

.

Declaration of interests

☐ X The authors declare that they have no known competing financial interests or personal relationships that could have appeared to influence the work reported in this paper.

The authors declare the following financial interests/personal relationships which may be considered as potential competing interests:

Declaration of interests

☐ X The authors declare that they have no known competing financial interests or personal relationships that could have appeared to influence the work reported in this paper.

The authors declare the following financial interests/personal relationships which may be considered as potential competing interests:
